Cycler and Self-Cycler Orbits using Solar Sails

Harry Holt*[(1)], Dario Izzo[(1)], Chit Hong Yam[(2)], and Zhong Zhang[(3)]

[(1)]Advanced Concepts Team, European Space Research and Technology Centre, ESA, Noordwijk, The Netherlands
[(2)]Space Mission Design Specialist, Tokyo, Japan
[(3)]Department of Aerospace Science and Technology, Politecnico di Milano, Milan, 20156, Italy

***Abstract* - Solar sails provide continuous, propellant-free thrust that expands the design space of cycler orbits beyond purely ballistic solutions. In this work, we develop a framework for optimising solar sail cyclers using a multi-gravity-assist model. Rather than solving a specific transfer, which may yield an infeasible optimal control problem, we instead treat sail performance as a decision variable and compute the minimum level required to guarantee the existence of a prescribed cycler. This reformulation converts the problem into a well-posed nonlinear program. The approach is applied to transfers in the solar system as well as the fictitious Altaira system, demonstrating both *multi-body cyclers* and *self-cyclers*. Results show that the proposed method systematically characterises the feasible cycler design space and enables straightforward tuning of encounter frequency and relative velocity.**

I. Introduction

Ballistic cycler orbits, such as the Aldrin-type Earth-Mars cycler and resonant Earth-return orbits, have long been proposed as transportation networks for sustained cargo logistics within the solar system [1, 2, 3, 4]. These trajectories rely on idealised multi-body resonances and carefully phased gravity assists, with little flexibility beyond the highly constrained natural gravitational dynamics.

Solar sails provide continuous, propellant-free thrust that fundamentally alters the solution space, enabling families of cycler orbits that either generalise ballistic solutions or are infeasible under purely ballistic dynamics. The existence of such solar sail cyclers for circular-coplanar orbits was identified by Stevens and Ross [5, 6], and has been extended to up to four cycles in [7]. Indeed, it is well known that solar sails can help establish non-Keplerian orbits [8, 9, 10] and even multi-reversal orbits [11].

Systematic approaches to designing ballistic cycler orbits [12, 13, 14, 15, 16] and solar sail stop-over cyclers [17, 18] exist. As mentioned, preliminary work also exists for circular-coplanar solar sail cycler orbits [7]. However, a general framework for identifying and characterizing sail-enabled cycler geometries beyond circular-coplanar orbits is missing. To build on these works, we explore the design space of solar sail cycler orbits between both single- and multiple bodies.

To search and characterise solar sail cyclers, we formulate the problem as a reachability problem [19], where the objective is to find the minimum solar sail strength required to make a given transfer feasible. By treating sail performance as a decision variable, the resulting formulation defines a well-posed nonlinear program and avoids the infeasibilities and numerical ill-conditioning that can arise when sail properties are fixed a priori. The model adopts a multi-gravity-assist structure with solar sail legs, which are transcribed using a forward–backward zero-order hold (ZOH) construction with variable-time segments [20]. The solar sail is modelled with ideal reflectivity, parametrised by its lightness number and cone and clock angles [8]. The gravity assists are modelled using the patched-conic approximation, neglecting the time spent inside the planet's sphere of influence. The framework allows the timing and parameters of each gravity assist to vary freely, enabling simultaneous optimisation across multiple planet-to-planet segments. The objective is to minimise the sail lightness number while optionally targeting a prescribed relative flyby velocity.

The paper is structured as follows. We first introduce the dynamical model and formulate the associated trajectory optimisation problem. Analytical gradients for the mismatch constraints, planetary flybys, and variable-segment formulation are then derived. In Section III, we apply our framework to both *self-cycler* and *multi-body cycler* orbits in our solar system and the artificial solar

*Email: harry.holt@esa.int

system from the GTOC 13 problem [21]. For *self-cyclers*, we investigate the sail strength required to revisit the same planet multiple times per orbital period, with at least a certain target relative velocity. The *multi-body cyclers* section, on the other hand, aims to minimise relative velocity. As such, we start from the special case of an instantaneous stop-over cycler, and transition from here up to *near*-ballistic cyclers (such as the 7-cycle Aldrin-type cyclers). Finally, conclusions are presented in Section IV.

II. Problem Description

A. Multi-leg planetary flybys

Let us consider a multi-leg flyby transcription. A planetary sequence can be defined as

$$\mathcal{P} = \{P_0, P_1, \dots, P_{N_\ell}\},$$

with $N_\ell = |\mathcal{P}| - 1$ legs. The formulation is valid for generic planet sequences, including planetary revisits. For example, solving a trajectory from planet A to planet B and back to planet A would be $\{P_0^A, P_1^B, P_2^A\}$. Solving for the sequence of visits itself is a global optimisation problem and is not focus of this work. However, once the sequence is defined, there remains the challenging task of solving the trajectory between each node.

In this work, each leg is transcribed with a forward–backward ZOH_α construction [20] (using cut parameter $\alpha \in [0, 1]$ and n_{seg} segments per leg). The ZOH transcription begins by partitioning each leg into n_{seg} contiguous subintervals. Over each subinterval, the control is held constant.

The notation used throughout is:

k :	leg index, $k = 0, \dots, N_\ell - 1$,
i :	segment index within leg k, $i = 0, \dots, n_{\mathrm{seg}} - 1$,
α :	forward–backward cut parameter of ZOH_α,
β :	solar sail lightness number,
$\alpha_{s,k,i}$:	cone angle on segment (k, i),
$\beta_{s,k,i}$:	clock angle on segment (k, i),
t_k :	planetary encounter time at P_k,
$\Delta t_{k,i}$:	segment duration within leg k,
$w_{k,i}$:	softmax variable for segment (k, i).

B. Solar sail dynamics

The solar sail dynamics are given by:

$$\begin{cases} \dot{\boldsymbol{r}} = \boldsymbol{v} \\ \dot{\boldsymbol{v}} = -\frac{\mu}{r^3}\boldsymbol{r} - b\,\kappa\left(\frac{r_0}{r}\right)^2(\hat{\mathbf{u}}_n \cdot \hat{\mathbf{u}}_r)^2\hat{\mathbf{u}}_n \end{cases} \tag{1}$$

where $\kappa = 2\frac{CA}{m}$ is the maximum acceleration due to the solar sail at r_0 and is directly proportional to the sail area A, the solar flux at $r_0 = 1$ AU, C, and inversely proportional to the spacecraft mass m. $b \geq 0$ is an optimisation variable to control the strength of the sail. This is similar to [18] and [19], where the latter formulates the problem with an indirect method. The lightness number characterises the relative strength of the solar sail compared to the gravitational acceleration:

$$\beta = \frac{a_{\mathrm{sail}}}{a_{\mathrm{grav}}} = \frac{2bCA}{m}\frac{r_0^2}{\mu}. \tag{2}$$

The sail-normal orientation is parametrised by two angles $\alpha_{s,k,i}$ and $\beta_{s,k,i}$ in the local orthonormal frame $\{\hat{\boldsymbol{u}}_r, \hat{\boldsymbol{u}}_t, \hat{\boldsymbol{u}}_h\}$, defined by

$$\hat{\boldsymbol{u}}_r = \frac{\boldsymbol{r}}{\|\boldsymbol{r}\|}, \qquad \hat{\boldsymbol{u}}_h = \frac{\boldsymbol{r} \times \boldsymbol{v}}{\|\boldsymbol{r} \times \boldsymbol{v}\|}, \qquad \hat{\boldsymbol{u}}_t = \hat{\boldsymbol{u}}_h \times \hat{\boldsymbol{u}}_r,$$

and

$$\begin{aligned} \hat{\boldsymbol{u}}_n(\alpha_{s,k,i}, \beta_{s,k,i}) = \cos\alpha_{s,k,i}\,\hat{\boldsymbol{u}}_r + \sin\alpha_{s,k,i}\sin\beta_{s,k,i}\,\hat{\boldsymbol{u}}_t \\ + \sin\alpha_{s,k,i}\cos\beta_{s,k,i}\,\hat{\boldsymbol{u}}_h. \end{aligned} \tag{3}$$

Hence,

$$\hat{\boldsymbol{u}}_n \cdot \hat{\boldsymbol{u}}_r = \cos\alpha_{s,k,i}.$$

C. Optimisation Problem

The corresponding nonlinear program can be stated as

$$\begin{aligned} \text{find: } & b,\ \alpha_{s,k,i},\ \beta_{s,k,i}, \\ & v_k^-,\ \hat{\boldsymbol{d}}_k^-,\ v_k^+,\ \hat{\boldsymbol{d}}_k^+, \\ & T_k,\ w_{k,i},\ t_0, \\ \text{minimise: } & b, \\ \text{subject to: } & b \geq 0, \\ & 0 \leq \alpha_{s,k,i} \leq \pi/2, \\ & \boldsymbol{mc}_\alpha^{(k)} = \boldsymbol{0}, \quad k = 0, \dots, N_\ell - 1, \\ & \text{Flyby constraints Eqs. (6)–(9)}, \\ & \sum_{k=0}^{N_\ell - 1} T_k \leq T_{\max}, \\ & v_{\infty,\mathrm{target}}^{\mathrm{lower}} \leq v_k^+, v_k^- \leq v_{\infty,\mathrm{target}}^{\mathrm{upper}} \end{aligned} \tag{4}$$

where $\boldsymbol{v}_{\infty,k}^+ = v_k^+\hat{\boldsymbol{d}}_k^+$ are outgoing hyperbolic-excess variables at node $k = 0, \dots, N_\ell - 1$, and $\boldsymbol{v}_{\infty,k}^- = v_k^-\hat{\boldsymbol{d}}_k^-$ are incoming hyperbolic-excess variables at node $k = 1, \dots, N_\ell$. Here, $\boldsymbol{mc}_\alpha^{(k)}$ denotes the mismatch constraints on leg k, and the flyby constraints are those given in Eqs. (6)–(9). Two additional inequality constraints are imposed: an upper bound on the total time of flight $T_{\max}$ and lower/upper bounds on the target flyby velocities $v_{\infty,\mathrm{target}}^{\mathrm{lower}}$ and $v_{\infty,\mathrm{target}}^{\mathrm{upper}}$. A visualisation of the scheme is given in Figure 1.

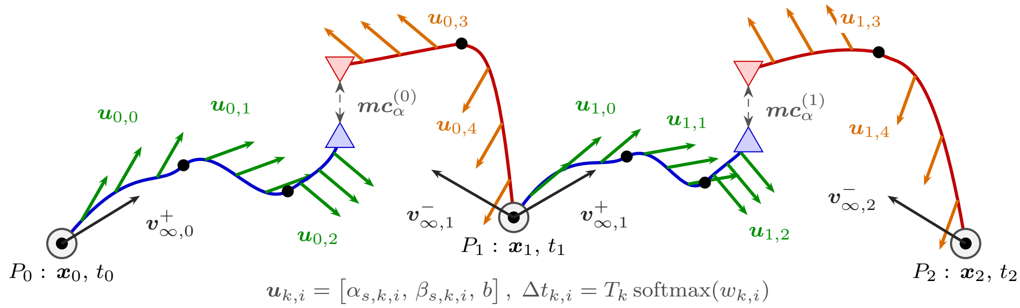

Fig. 1: Three-planet sequence with piecewise-constant (ZOH) control on each leg. The time encounter of each planet, along with the duration of each segment is free to vary. The flyby constraints on magnitude and direction are equality and inequality constraints respectively.

D. The mismatch constraints

For each leg k, the equality constraints are denoted by $\boldsymbol{mc}_\alpha^{(k)}$ and are referred to as *mismatch constraints*. Their construction is governed by the cut parameter $\alpha \in [0,1]$, which partitions the n_{seg} segments of leg k into

$$n_{\text{fwd}} = \lfloor \alpha n_{\text{seg}} \rfloor, \qquad n_{\text{bck}} = n_{\text{seg}} - n_{\text{fwd}}.$$

Let $\boldsymbol{x}_{\text{fwd}}^{(k)}$ denote the state obtained by forward propagation from P_k over the first n_{fwd} segments with controls $\boldsymbol{u}_{k,i}$, and let $\boldsymbol{x}_{\text{bck}}^{(k)}$ denote the state obtained by backward propagation from P_{k+1} over the remaining n_{bck} segments with reversed controls. The mismatch constraints are defined as

$$\boldsymbol{mc}_\alpha^{(k)} \triangleq \boldsymbol{x}_{\text{bck}}^{(k)} - \boldsymbol{x}_{\text{fwd}}^{(k)}, \qquad k = 0, \dots, N_\ell - 1, \tag{5}$$

and enforced through $\boldsymbol{mc}_\alpha^{(k)} = \boldsymbol{0}$. This imposes $\mathcal{C}^0$ continuity at the forward–backward junction of each leg. The limiting cases $\alpha = 1$ and $\alpha = 0$ recover purely forward and purely backward shooting, respectively.

E. Planetary flyby model

At each intermediate encounter node, we adopt the standard impulsive gravity-assist model in the Milankovic sense: the flyby is assumed instantaneous, with no powered manoeuvre at periapsis and no change in the magnitude of the hyperbolic excess speed.

Let $\boldsymbol{v}_{\infty,k}^-$ and $\boldsymbol{v}_{\infty,k}^+$ denote, respectively, the incoming and outgoing hyperbolic excess velocity vectors at intermediate node $k = 1, \dots, N_\ell - 1$. They satisfy

$$\|\boldsymbol{v}_{\infty,k}^-\|^2 - \|\boldsymbol{v}_{\infty,k}^+\|^2 = 0. \tag{6}$$

The turning geometry is bounded by the minimum allowed periapsis radius $r_{p,k}^{\min}$ and planetary gravitational parameter μ_k. Throughout this work $r_{p,k}^{\min} = 1.1 R_k$ where R_k is the planetary radius. Defining

$$e_{\min,k} = 1 + \frac{r_{p,k}^{\min}}{\mu_k}\,\|\boldsymbol{v}_{\infty,k}^-\|^2, \tag{7}$$

the maximum admissible turning angle satisfies

$$\cos\delta_{\max,k} = 1 - \frac{2}{e_{\min,k}^2}. \tag{8}$$

Hence the flyby feasibility constraint can be written as

$$\cos\delta_{\max,k} - \frac{\boldsymbol{v}_{\infty,k}^- \cdot \boldsymbol{v}_{\infty,k}^+}{\|\boldsymbol{v}_{\infty,k}^-\|\,\|\boldsymbol{v}_{\infty,k}^+\|} \le 0. \tag{9}$$

Equations (6)–(9) provide, for each intermediate planet, one equality and one inequality flyby constraint. This formulation avoids having to take an arccos or arcsin, whose derivatives become singular near the boundaries of their domains, leading to poorly conditioned gradients.

F. The time grid

We adopt a variable time grid parameterised via the softmax transformation [20]. For each leg k, define $T_k = t_{k+1} - t_k$ and introduce $\boldsymbol{w}_k \in \mathbb{R}^{n_{\text{seg}}}$. The normalised segment fractions are

$$\sigma_{k,i} \triangleq \frac{e^{w_{k,i}}}{\sum_{j=0}^{n_{\text{seg}}-1} e^{w_{k,j}}}, \qquad i = 0, \dots, n_{\text{seg}} - 1,$$

so that $\sum_i \sigma_{k,i} = 1$ is satisfied identically. The physical segment durations are

$$\Delta t_{k,i} = T_k\,\sigma_{k,i}, \qquad i = 0, \dots, n_{\text{seg}} - 1,$$

and the grid nodes are recovered recursively as

$$t_{k,0} = t_k, \quad t_{k,i+1} = t_{k,i} + \Delta t_{k,i}, \quad i = 0, \dots, n_{\text{seg}} - 1.$$

This parameterisation guarantees strict positivity $\Delta t_{k,i} > 0$, enforces normalisation without additional affine constraints, and provides a smooth map suited to gradient-based nonlinear programming.

G. The Gradients

For each leg k, the mismatch vector is $\boldsymbol{mc}_\alpha^{(k)} \in \mathbb{R}^6$. The variational integration over the forward and backward sub-arcs provides the Jacobian blocks

$$\frac{\partial \boldsymbol{mc}_\alpha^{(k)}}{\partial \boldsymbol{x}_0^{(k)}}, \qquad \frac{\partial \boldsymbol{mc}_\alpha^{(k)}}{\partial \boldsymbol{x}_1^{(k)}}, \qquad \frac{\partial \boldsymbol{mc}_\alpha^{(k)}}{\partial \boldsymbol{u}_{k,i}}, \qquad \frac{\partial \boldsymbol{mc}_\alpha^{(k)}}{\partial t_{k,i}},$$

where $\boldsymbol{x}_0^{(k)}$ and $\boldsymbol{x}_1^{(k)}$ are the leg boundary states, $\boldsymbol{u}_{k,i} = [\alpha_{s,k,i}, \beta_{s,k,i}, b]$ are the segment controls, and $t_{k,i}$ are the in-leg grid nodes. For brevity, we skip the full derivation of these Jacobian blocks and instead the reader is referred to [20], where a thorough explanation of these mismatch constrain gradients can be found.

However, the addition of the gravitational flybys needs to be considered here. The leg-boundary velocities contain the hyperbolic-excess terms:

$$\boldsymbol{v}_0^{(k)} = \dot{\boldsymbol{r}}_{P_k}(t_k) + \boldsymbol{v}_{\infty,k}^{+}, \qquad \boldsymbol{v}_1^{(k)} = \dot{\boldsymbol{r}}_{P_{k+1}}(t_{k+1}) + \boldsymbol{v}_{\infty,k+1}^{-}.$$

Hence, by chain rule,

$$\frac{\partial \boldsymbol{mc}_\alpha^{(k)}}{\partial \boldsymbol{v}_{\infty,k}^{+}} = \left(\frac{\partial \boldsymbol{mc}_\alpha^{(k)}}{\partial \boldsymbol{x}_0^{(k)}}\right)_{(:,4:6)}, \frac{\partial \boldsymbol{mc}_\alpha^{(k)}}{\partial \boldsymbol{v}_{\infty,k+1}^{-}} = \left(\frac{\partial \boldsymbol{mc}_\alpha^{(k)}}{\partial \boldsymbol{x}_1^{(k)}}\right)_{(:,4:6)}.$$

If each block is parametrised as $\boldsymbol{v}_{\infty,k}^{+} = v_k^{+} \hat{\boldsymbol{d}}_k^{+}$ and $\boldsymbol{v}_{\infty,k}^{-} = v_k^{-} \hat{\boldsymbol{d}}_k^{-}$, then, for $s \in \{+,-\}$,

$$\frac{\partial \boldsymbol{v}_{\infty,k}^{s}}{\partial v_k^{s}} = \hat{\boldsymbol{d}}_k^{s}, \qquad \frac{\partial \boldsymbol{v}_{\infty,k}^{s}}{\partial \hat{\boldsymbol{d}}_k^{s}} = v_k^{s}\, \mathbf{I}_3,$$

which gives the gradients with respect to v_k^s and $\hat{\boldsymbol{d}}_k^s$ directly.

For controls, the per-segment Jacobian $\partial \boldsymbol{mc}_\alpha^{(k)}/\partial \boldsymbol{u}_{k,i}$ gives derivatives with respect to $\alpha_{s,k,i}$ and $\beta_{s,k,i}$ from the first two columns. Since b is global and appears in every segment control block, its gradient is accumulated as

$$\frac{\partial \boldsymbol{mc}_\alpha^{(k)}}{\partial b} = \sum_{i=0}^{n_{\text{seg}}-1} \left(\frac{\partial \boldsymbol{mc}_\alpha^{(k)}}{\partial \boldsymbol{u}_{k,i}}\right)_{(:,3)}.$$

Time derivatives are obtained in two layers. Node-time sensitivity enters through planetary ephemerides at each boundary epoch t_k:

$$\frac{d\boldsymbol{x}_{P_k}}{dt_k} = \begin{bmatrix} \dot{\boldsymbol{r}}_{P_k} \\ \dot{\boldsymbol{v}}_{P_k} \end{bmatrix},$$

with node epochs defined by

$$t_k = t_0 + \sum_{q=0}^{k-1} T_q, \qquad k = 0, \ldots, N_\ell,$$

so that

$$\frac{\partial t_k}{\partial t_0} = 1, \quad \frac{\partial t_k}{\partial T_q} = \mathbf{1}_{\{q<k\}}, \quad t_f = t_{N_\ell}.$$

which contributes to $\partial \boldsymbol{mc}_\alpha^{(k)}/\partial t_k$ and $\partial \boldsymbol{mc}_\alpha^{(k)}/\partial t_{k+1}$ through $\partial \boldsymbol{mc}_\alpha^{(k)}/\partial \boldsymbol{x}_0^{(k)}$ and $\partial \boldsymbol{mc}_\alpha^{(k)}/\partial \boldsymbol{x}_1^{(k)}$. Second, in-leg grid sensitivities are propagated via $\partial \boldsymbol{mc}_\alpha^{(k)}/\partial t_{k,i}$.

With softmax time encoding, for leg k with TOF T_k and logits $\boldsymbol{w}_k \in \mathbb{R}^{n_{\text{seg}}}$, the softmax weights are

$$\sigma_{k,i} = \frac{e^{w_{k,i}}}{\sum_{j=0}^{n_{\text{seg}}-1} e^{w_{k,j}}},$$

$$t_{k,i} = t_k + \sum_{p=0}^{i-1} T_k\, \sigma_{k,p}, \qquad i = 1, \ldots, n_{\text{seg}}.$$

so that

$$\frac{\partial t_{k,i}}{\partial T_k} = \sum_{p=0}^{i-1} \sigma_{k,p},$$

$$\frac{\partial t_{k,i}}{\partial w_{k,j}} = T_k \sum_{p=0}^{i-1} \frac{\partial \sigma_{k,p}}{\partial w_{k,j}},$$

$$\frac{\partial \sigma_{k,p}}{\partial w_{k,j}} = \sigma_{k,p}(\delta_{pj} - \sigma_{k,j}).$$

These relations provide mismatch gradients with respect to initial time, intermediate node times, final time, flyby velocities $\boldsymbol{v}_{\infty,k}$, and the sail controls $[\alpha_{s,k,i}, \beta_{s,k,i}]$ and strength b.

III. Experimental Setup and Results

A. Problem Data

In this work we consider three systems: a *simple* circular, coplanar solar system; an eccentric and inclined *solar* system (closer to full ephemeris); and the *altaira* system from *GTOC 13*. The parameters for these systems, and the planets therein, are given in Tables 1 and 2. For reference, information on the IKAROS [22], NEA scout [23], LightSail2 [24] and GTOC 13 [21] sails are also given. Note that in the *simple* model, the semi-major axis and hence period of Mars has been adjusted such that exactly 8 orbits occur every 15 years. This is standard in the literature (e.g. [13]) and means the synodic period repeats 7 times and the resulting geometry repeats exactly every 15 years.

Tab. 1: System constants used in each model, along with some example solar sail parameters.

System	$\mu_\star$ [km^3/s^2]	C [N/m^2]	r_0 [AU]
Simple	1.32712e11	4.5600e-6	1
Solar	1.32712e11	4.5600e-6	1
Altaira	1.39348e11	5.4026e-6	1
Sail	**A [m^2]**	**M [kg]**	**β**
IKAROS	196	307	9.819e-4
NEA Scout	86	14	9.447e-3
LightSail2	32	4.93	9.982e-3
GTOC 13	15000	500	5.206e-2

B. Self-cyclers

Self-cyclers involve a single planet that is revisited multiple times per orbit period. We parametrise with two variables: the number of revisits per orbit, N_ℓ, and a lower bound on the target flyby velocity $v_{\infty,\text{target}}^{\text{lower}}$. Hence the upper bound is not constrained, $v_{\infty,\text{target}}^{\text{upper}} = \infty$. We only consider one orbital period the maximum allowed time of flight, $T_{\max}$, as the system then repeats. The lower bound on the target flyby velocity is present to prevent the trivial solution of co-orbiting with the planet when $v_{\infty,\text{target}} = 0$ km/s. Two other trivial solutions exist: when one revisit is desired, an intersecting orbit with the same period can achieve this ballistically; when two revisits are desired, the same orbital shape at a different inclination can achieve many different relative flyby velocities at the node crossings. As validation, our method converges on these solutions when present, but these are left out of the plots and discussion below. A potential motivation for maintaining a higher relative velocity could be for easier departure from the planet or to maintain a regular revisit to a sunward co-rotating point, such as the L1 point.

Figure 2 summarises how sail strength varies across revisit count and $v_{\infty,\text{target}}$ settings. The left column shows the minimum feasible lightness number for each revisit and $v_{\infty,\text{target}}$. A lower value indicates easier-to-realise cyclers for the same mission geometry. The right column provides representative trajectories at selected grid points. As expected, as both the number of revisits and the relative velocity increase, so does the required sail strength. The sail needs to counteract the kick provided by the flyby. As seen in the altitude plots (right column), the solar sail trajectory is always inside the planetary orbit. This approach also works in a circular model, where it shares many similarities with quasi-periodic solar sail orbits in the circular restricted three-body problem. However, here we use a two-body and zero sphere-of-influence model. Whilst this has its limitations, it is nonetheless interesting as it can be easily used for eccentric orbits. Venus requires a smaller sail despite the time for revisit being smaller, as the solar radiation pressure is stronger closer to the star. Eden is also shown to confirm that the methodology works across different stellar flux and gravitational parameter models. Finally, although the total time of flight is an inequality constraint, it is pushed to equality for all cases as revisiting the planet more often requires a stronger sail.

C. Multi-body Cyclers

Unlike *self-cyclers*, where we had a lower bound on the target $v_{\infty,\text{target}}$, the objective for *multi-body cyclers* is reversed. *Near*-ballistic solutions exist with high relative velocities, whilst impulsive manoeuvres [13, 14, 15, 25] and low-thrust propulsion [26, 25] or solar sails [17, 18, 7, 27] are used to either minimise the v_∞ or reduce the time-of-flight between planetary encounters. Thus, in this section we use $v_{\infty,\text{target}}^{\text{lower}} = 0$ km/s and only $v_{\infty,\text{target}}^{\text{upper}}$ is active. A wide range of cycler trajectories with varying encounter velocities, transfer times, and repeat periods has been identified in the literature. In this work, however, we focus on cyclers whose minimum component $(P^A \to P^B \to P^A)$ completes within a single synodic period, T_{synodic}. Thus, we define an n_{pairs}-synodic-period $A-B$ cycler as $(P^A \to P^B)^{n_{\text{pairs}}} \to P^A$, with a maximum allowable time of flight set to $T_{\max} = n_{\text{pairs}} T_{\text{synodic}}$. No additional symmetry constraints are imposed, and the methodology should therefore remain applicable to a broad class of *multi-body cyclers*.

In [13], a near-ballistic 7-synodic-period aldrin-type Earth–Mars cycler is presented for the circular coplanar model. Whilst in a zero sphere-of-influence model this cycler is ballistic (with the additional limitation of no flyby deflection at Mars), it requires a turning angle (83.67°) that can only be achieved with a periapsis inside the Earth's surface. As such, they term it near-ballistic. Restricting the minimum flyby altitude to $r_p = R_k + 200$ km $\approx 1.03136 R_k$ requires 1350.3 m/s per flyby to realise (equivalently 1420.0 m/s for $r_p = 1.05 R_k$ and 1600.5 m/s for $r_p = 1.1 R_k$). An objective in this section is to find the minimum sail strength required to make such a cycler feasible.

At the other end of the scale are solar sail stop-over cyclers [17, 18]. The fact that these cyclers rendezvous with the target planet has two advantages. Firstly, they are easier to meet logistically, since there is no velocity mismatch between the cycler spacecraft and a spacecraft in orbit around the target planet. Secondly, the ability to wait at the target planet relaxes the usually

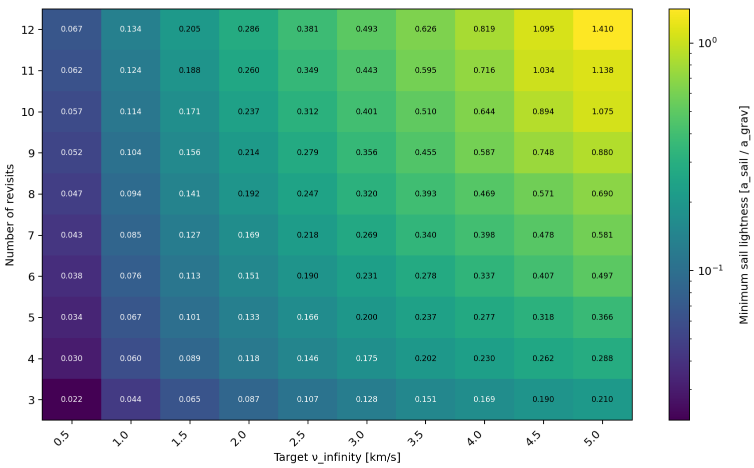

(a) Earth *self-cycler* heatmap

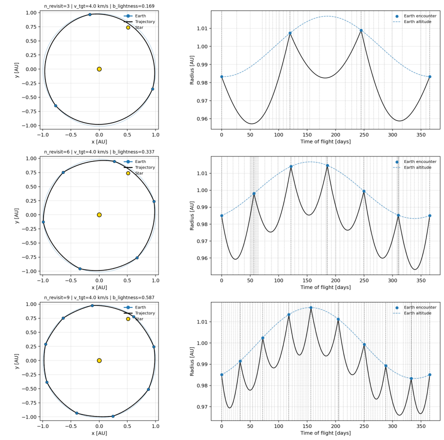

(b) Earth example solutions

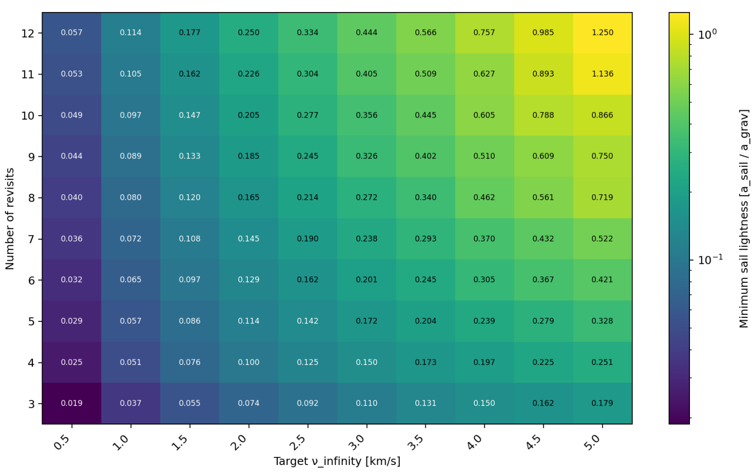

(c) Venus *self-cycler* heatmap

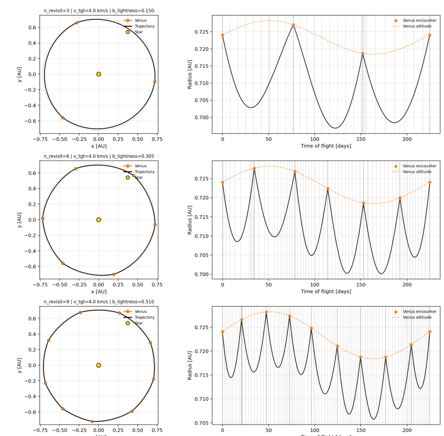

(d) Venus example solutions

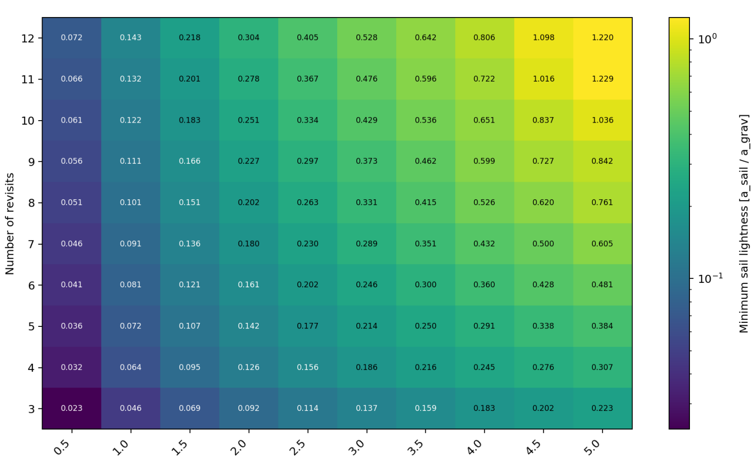

(e) Eden *self-cycler* heatmap

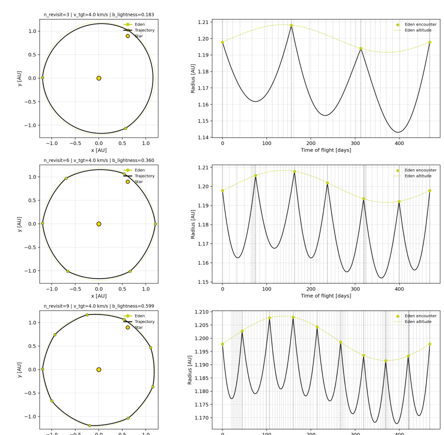

(f) Eden example solutions

Fig. 2: Self-cycler summary: left column = minimum-β heatmaps, right column = representative example columns, for Earth, Venus in the *solar* model and Eden in the *altaira* model (top to bottom).

Tab. 2: Planetary parameters used in each model.

System	Planet	μ_k $[km^3/s^2]$	R_k $[km]$	Initial Epoch [YY-MM-DD HH:MM:SS]	a AU	e -	i rad	Ω rad	ω rad	ν rad
Simple	Earth	3.98600e5	6378.0	2000-01-01 00:00:00	1.00000	0	0	-	-	-5.07716e-02
	Mars	4.28280e4	3397.0	2000-01-01 00:00:00	1.5206	0	0	-	-	-1.07259
Solar	Venus	3.24859e5	6052.0	2000-01-01 00:00:00	0.723337	0.00676604	0.0592447	1.33706	0.959853	2.54619
	Earth	3.98600e5	6378.0	2000-01-01 00:00:00	1.00000	1.66998e-02	-5.90174e-05	0	1.79807	-5.07716e-02
	Mars	4.28280e4	3397.0	2000-01-01 00:00:00	1.52372	0.0934146	0.0322463	0.863649	-1.27953	-1.07259
Altaira	Yavin	6.36304e6	18013.2	0	0.859158	0.0500000	0.0523599	1.92857	2.58544	2.75018
	Eden	4.43854e5	6697.4	0	1.20000	0.00700000	0.0174533	1.87574	6.21700	0.916850

highly constrained flight windows, allowing the mission analysts to wait until better phasing exists between the two planets. Thus, an additional parameter in the form of a waiting time is usually introduced in the literature which only exists in this special case of $v_{\infty,target}^{\text{upper}} = 0$ km/s. Although this reduces the lightness number required to realise the cycler, we avoid doing so, as it no longer applies for $v_{\infty,target}^{\text{upper}} > 0$ km/s. Nonetheless, we found problems with $v_{\infty,target}^{\text{upper}} = 0$ km/s to be much better behaved and easier to converge and, as is shown in the remainder of this section, they can then be used to transition to *near*-ballistic cyclers.

Our approach involves two steps: extending cyclers from 2-cycles up to $N_{\text{pairs}}^{\text{max}}$-cycles for the special case of the instantaneous stop-over cycler ($v_{\infty,target}^{\text{upper}} = 0$), and then continuing across $v_{\infty,target}^{\text{upper}}$ for each planet until the unconstrained cycler is recovered.

1. Extending instantaneous stop-over cyclers

Solving Algorithm 1 implements an extension strategy that increases cycler length gradually, using the best previously found solution as an initial guess for the next. For each value of n_{pairs}, the multi-start loop explores local perturbations around the warm start solution and the best feasible candidate is promoted to the next extension level. Figure 3 shows this process starting from $n_{\text{pairs}} = 2$ to $n_{\text{pairs}} = 5$ for the *simple* Earth-Mars instantaneous stop-over cycler. Note that we restrict each n_{pairs}-synodic-period cycler to be within $T_{\max} = n_{\text{pairs}} T_{\text{synodic}}$. For the *simple* Earth-Mars case this results in a sail lightness number of $\beta = 0.301$.

Whilst it would be ideal to solve for $N_{\text{pairs}}^{\text{max}}$ directly, doing so is also a global optimisation problem. The interested reader is referred to [14] among others for such work. Whilst this extension approach is local, it keeps the search stable as dimensionality grows and provides a consistently good solution. Future work will aim to investigate how to transition to different families of cycler orbits.

2. $v_{\infty,target}$ continuation

Now that we have a solution for the instantaneous stop-over cyclers, namely $(v_{\infty,target}^{A}, v_{\infty,target}^{B}) = (0, 0)$, we can start solving for different $(v_{\infty,target}^{A}, v_{\infty,target}^{B})$ pairs. Since $v_{\infty,target}$ is an upper bound, all solutions from grid points with values less than or equal to $v_{\infty,target}$ are also feasible, albeit potentially sub-optimal. As such, we can use $(i-1, j)$ or $(i, j-1)$ as an initial guess to solve for (i, j). We also add some small perturbations around these initial guesses for each of $\alpha_{s,k,i}$, $\beta_{s,k,i}$, v_k^-, $\hat{\boldsymbol{d}}_k^-$, v_k^+, $\hat{\boldsymbol{d}}_k^+$, T_k, $w_{k,i}$, t_0 to prevent the solver from getting stuck, again using a multi-start approach with $N_{\text{multi}} = 32$.

Figure 4 summarises how *multi-body cyclers* vary across target relative velocities at the two planetary flybys for $n_{\text{pairs}} = 7$ (Earth-Mars) and $n_{\text{pairs}} = 8$ (Eden-Yavin) synodic period cyclers. The left column shows the minimum feasible lightness number for a given upper bound $(v_{\infty,target}^{A}, v_{\infty,target}^{B}) = (i, j)$ pair. Again, lower values indicate easier-to-realise cyclers. The bottom left corner corresponds to the instantaneous stop-over cycler, whilst the top right corner is the *near*-ballistic solution. It is clear that $\beta_{i,j} \le \beta_{i-1,j}$ and $\beta_{i,j} \le \beta_{i,j-1}$. This is nice validation that our technique correctly minimises the sail strength. The right column panels provide representative trajectories at selected operating points.

Comparing *simple* Earth-Mars and *solar* Earth-Mars results, it becomes apparent that the eccentricity increases the necessary sail strength β for different target flyby velocities. The region near $(v_{\infty,target}^{\text{Earth}}, v_{\infty,target}^{\text{Mars}}) \ge (6.0, 10.0)$ have $\beta = 0.0055$ for the *simple* model and essentially become unconstrained, as further increasing $v_{\infty,target}^{\text{upper}}$ for either planet do not reduce the necessary sail strength. However, the sail strength increases to $\beta = 0.022$ for the *solar* model primarily due to the eccentricity of Mars' orbit. It is noted that we fixed the initial epoch to $0 < t_0 < T_{\text{synodic}}$. In [13] the near-ballistic 7-synodic-period Earth-Mars cycler is found to minimise the required Δv launching in August 2003, which is outside our initial epoch bounds. Future work can investi-

Algorithm 1 *Multi-body cycler* solar sail ZOH cycler-extension with nested multi-start loop.

Input: target sequence $\mathcal{P} = \{P_0, P_1, \ldots, P_{N_\ell}\}$, $N_{\text{multi}} = 32$, $N_{\text{pairs}}^{\max} = (N_\ell - 1)/2$, $T_{\max}, \Delta T = T_{\max}/(2N_{\text{pairs}}^{\max})$
Initialise best_solutions $\leftarrow \{\}$
for $n_{\text{pairs}} = 2$ to $N_{\text{pairs}}^{\max}$ **do**
    Assign flyby chain: $(P^A \to P^B)^{n_{\text{pairs}}} \to P^A$
    Build cumulative time grid: $T_k^{(0)} \leftarrow k\,\Delta T, \quad k = 0, \ldots, 2n_{\text{pairs}}$
    if $n_{\text{pairs}} > 2$ **then**
        $x_{\text{prev}} \leftarrow$ best_solutions$[n_{\text{pairs}} - 1]$
        Copy shared variables for warm_start from x_{prev}: $\{v_k^-, \hat{\boldsymbol{d}}_k^-, v_k^+, \hat{\boldsymbol{d}}_k^+, T_k, w_{k,i}, t_0, \alpha_{s,k,i}, \beta_{s,k,i}, b\}$
        Initialise new-leg variables with $T_k^{(0)}$, $w_{k,i}$ and small initial $\alpha_{s,k,i}, \beta_{s,k,i}$
    else
        Build default warm_start from $T_k^{(0)}$, random flyby angles, and small initial $\alpha_{s,k,i}, \beta_{s,k,i}$, nominal b
    end if
    for $m_{\text{multi}} = 1$ to N_{multi} **do**
        Sample trial guess around warm_start
        Build Solar Sail ZOH Optimisation Problem and solve via IPOPT
        Store candidate trajectory and optimisation variables $\{v_k^-, \hat{\boldsymbol{d}}_k^-, v_k^+, \hat{\boldsymbol{d}}_k^+, T_k, w_{k,i}, t_0, \alpha_{s,k,i}, \beta_{s,k,i}, b\}$
    end for
    best_solutions$[n_{\text{pairs}}] \leftarrow \arg\min_m\, b$
end for

gate this approach across a range of t_0 values to further reduce the required sail strength.

For the *altaira* Eden-Yavin case, the sail strength required for the 8-synodic-period cycler is approximately half of the Earth-Mars case, at $\beta = 0.148$, however we dont find the same reduction in β as $v_{\infty,target}^{\text{upper}}$ increases, resulting in similar values of $\beta = 0.022$ for $\{v_{\infty,target}^{\text{Eden}}, v_{\infty,target}^{\text{Yavin}}\} \geq \{8.0, 9.0\}$. A clear symmetry is observed for the stop-over cycler, but this disappears for the higher relative velocities. Interestingly, the sail spends more time inside the orbit of the innermost planet (in this case Yavin) than it does for the Earth-Mars cycler, utilising the greater control authority enabled by the increased solar flux. This is likely because the 7-synodic-period cycler for *solar* Earth-Mars lasts 14.94 years, which is 5.30% of an orbital period from the geometry repeating itself. On the other hand, an 8-synodic-period Eden-Yavin cycler has a 29.5% error. Extending this to 9 synodic periods would reduce it to 16.83% but it is still further from repeating than the more symmetrical *solar* Earth-Mars cycler.

Finally, for comparison, a multi-impulsive transcription (MIT) using the same multi-leg flyby structure introduced in Section II for the ZOH_α formulation is also implemented, but where the continuous solar sail acceleration is replaced by discrete velocity impulses applied within each segment (at the segment midpoint in this setup). Using $n_{seg} = 5$ (segments per leg) gave a total Δv across 7-cycles of 999 m/s, compared to the $9,603$ m/s that would be required if an impulse was placed at each Earth-flyby during the *near*-ballistic Aldrin-type cycler mentioned in [13].[1]

IV. Conclusion

We apply our framework to study both *self-cycler* and *multi-body cycler* orbits in our solar system and the fictitious Altaira system in the GTOC 13 problem [21]. Self-cyclers, in which a single gravitational body is visited multiple times, are demonstrated for Earth, Venus and Eden, whilst *multi-body cyclers* are shown for Earth–Mars and Eden–Yavin. Our results show that sail-enabled cycler orbits exist across a range of lightness numbers and can be tuned for different frequency and v_∞ requirements, expanding the feasible cycler design space from *near*-ballistic cyclers to stop-over solar-sail concepts.

Future work will look to extend the *multi-body cyclers* to other families of *near*-ballistic cyclers with differing revisit times and repeats per synodic period. Another interesting avenue would be separating the sail strength required for the out-bound and in-bound legs, as done for stop-over cyclers in [18]. As for *self-cyclers*, the natural extension is to consider the link to solar sail enabled periodic orbits in the circular restricted three-body problem or similar.

[1] This ignores the potential of a powered flyby, which would further reduce the required Δv.

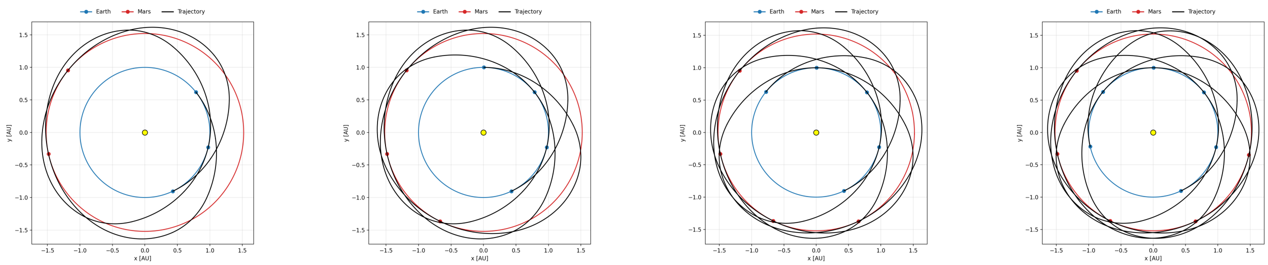

(a) $n_{\text{pairs}} = 2$ (b) $n_{\text{pairs}} = 3$ (c) $n_{\text{pairs}} = 4$ (d) $n_{\text{pairs}} = 5$

Fig. 3: *Simple* Earth-Mars instantaneous stop-over cycler ($v_{\infty,target}^{\text{upper}} = 0$) for different n_{pairs}, where each pair is extended from the previous solution. Each n_{pairs}-cycler is restricted to be within n_{pairs} synodic periods. The sail lightness number is $\beta = 0.301$.

References

[1] Hollister, W. M. “Periodic orbits for interplanetary flight.” Journal of Spacecraft and Rockets, Vol. 6, No. 4, pp. 366–369, 1969. doi:10.2514/3.29664. _eprint: https://doi.org/10.2514/3.29664.

[2] Hollister, W. M. and Menning, M. D. “Periodic swing-by orbits between earth and Venus.” Journal of Spacecraft and Rockets, Vol. 7, No. 10, pp. 1193–1199, 1970. doi:10.2514/3.30134. _eprint: https://doi.org/10.2514/3.30134.

[3] Hollister, W. and Rall, C. “Free-fall periodic orbits connecting earth and Mars.” “9th Aerospace Sciences Meeting,” doi:10.2514/6.1971-92. _eprint: https://arc.aiaa.org/doi/pdf/10.2514/6.1971-92.

[4] Byrnes, D. V., Longuski, J. M., and Aldrin, B. “Cycler orbit between Earth and Mars.” Journal of Spacecraft and Rockets, Vol. 30, No. 3, pp. 334–336, 1993. doi:10.2514/3.25519. _eprint: https://doi.org/10.2514/3.25519.

[5] Stevens, R. E. “Design of Optimal Cyclers Using Solar Sails.”

[6] Stevens, R. and Ross, I. M. “Preliminary Design of Earth-Mars Cyclers Using Solar Sails.” Journal of Spacecraft and Rockets, Vol. 42, No. 1, pp. 132–137, Jan. 2005. ISSN 0022-4650, 1533-6794. doi: 10.2514/1.2947.

[7] Rozhkov, M. and Starinova, O. “Cyclic Interplanetary Motion of a Cargo Solar Sail.” “Proceedings From The 6th International Symposium On Space Sailing (ISSS23),” 2023.

[8] McInnes, C. R. “Solar Sailing: Technology, Dynamics, and Mission Applications.” Springer Science & Business Media, 2004.

[9] Heiligers, J. “Non-Keplerian orbits using hybrid solar sail propulsion for Earth applications.”

[10] Heiligers, J., Macdonald, M., and Parker, J. S. “Design and Applications of Solar Sail Periodic Orbits in the Non-Autonomous Earth–Moon System.”

[11] Zeng, X., Alfriend, K. T., and Vadali, S. R. “Solar Sail Planar Multireversal Periodic Orbits.” Journal of Guidance, Control, and Dynamics, Vol. 37, No. 2, pp. 674–681, Mar. 2014. ISSN 0731-5090, 1533-3884. doi:10.2514/1.58598.

[12] McConaghy, T., Longuski, J., and Byrnes, D. “Analysis of a broad class of Earth-Mars cycler trajectories.” “AIAA/AAS Astrodynamics Specialist Conference and Exhibit,” p. 4420. 2002.

[13] Russell, R. P. and Ocampo, C. A. “Systematic Method for Constructing Earth-Mars Cyclers Using Free-Return Trajectories.” Journal of Guidance, Control, and Dynamics, Vol. 27, No. 3, pp. 321–335, 2004. doi:10.2514/1.1011. _eprint: https://doi.org/10.2514/1.1011.

[14] Russell, R. P. and Ocampo, C. A. “Global search for idealized free-return Earth-Mars cyclers.” Journal of Guidance, Control, and Dynamics, Vol. 28, No. 2, pp. 194–208, 2005.

[15] Russell, R. P. and Ocampo, C. A. “Optimization of a broad class of ephemeris model earth-mars cyclers.” Journal of Guidance, Control, and Dynamics, Vol. 29, No. 2, pp. 354–367, 2006.

[16] Pisarevsky, D. M., Kogan, A., and Guelman, M. “Interplanetary periodic trajectories in two-planet systems.” Journal of guidance, control, and dynamics, Vol. 31, No. 3, pp. 729–739, 2008.

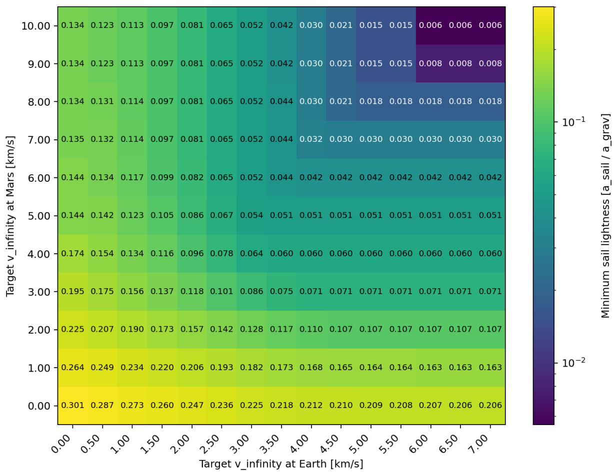

(a) *Simple* Earth-Mars *multi-body cycler* heatmap

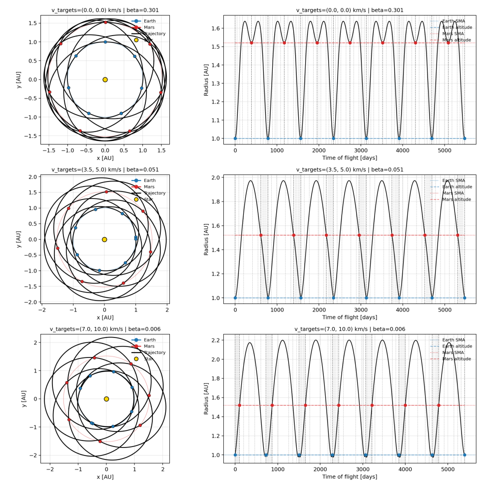

(b) *Simple* Earth-Mars example solutions

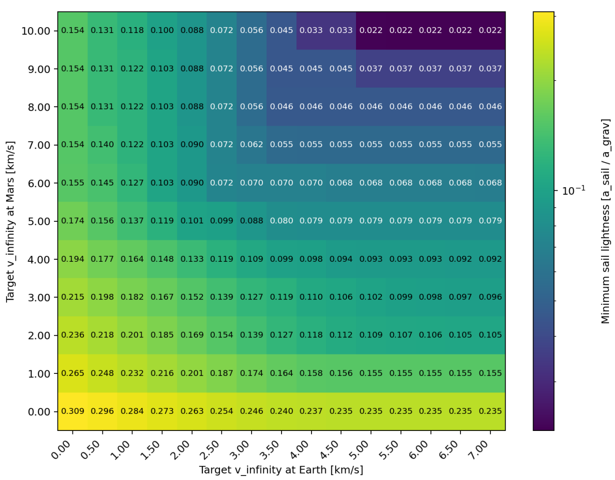

(c) *Solar* Earth-Mars *multi-body cycler* heatmap

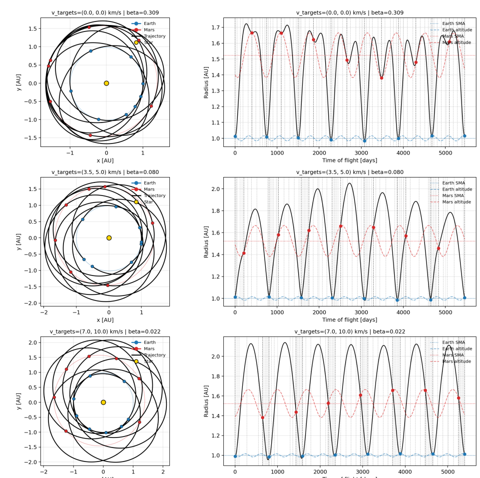

(d) *Solar* Earth-Mars example solutions

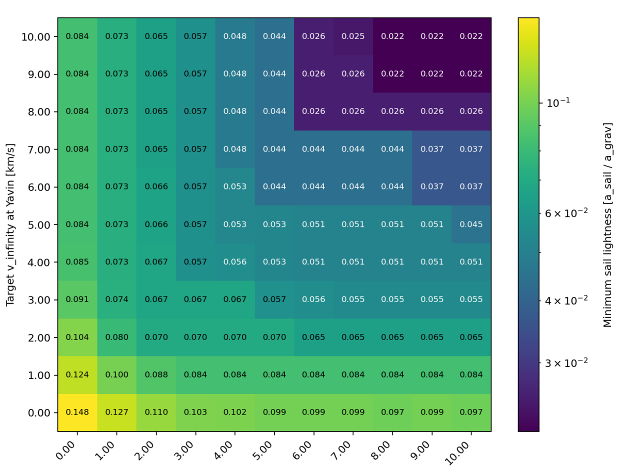

(e) *Altaira* Eden-Yavin *multi-body cycler* heatmap

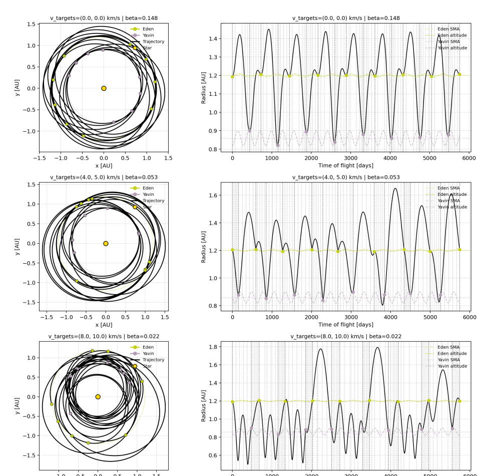

(f) *Altaira* Eden-Yavin example solutions

Fig. 4: Multi-body cyclers: left column = minimum-β heatmaps, right column = examples, in the *simple*, *solar* and *altaira* models for 7− and 8−synodic period cyclers. The initial epoch is bounded within $0 \leq t_0 \leq T_{\text{synodic}}$.

[17] Mengali, G. and Quarta, A. A. “Solar-Sail-Based Stopover Cyclers for Cargo Transportation Missions.” Journal of Spacecraft and Rockets, Vol. 44, No. 4, pp. 822–830, Jul. 2007. ISSN 0022-4650, 1533-6794. doi:10.2514/1.24423.

[18] Miguel, N., Colombo, C., and Vedova, F. D. “Systematic Construction of Solar-Sail-Based Stopover Cyclers.” The Journal of the Astronautical Sciences, Vol. 70, No. 2, p. 6, Mar. 2023. ISSN 2195-0571. doi:10.1007/s40295-023-00372-0.

[19] Acciarini, G., Izzo, D., and Zhang, Z. “Reachability for Low-Thrust Trajectories via Maximum Initial Mass.” arXiv preprint arXiv:2605.23770, 2026.

[20] Izzo, D., Holt, H., Acciarini, G., Beauregard, L., and Shimane, Y. “A practical guide to implementing zero-order-hold interplanetary trajectory legs.” arXiv preprint arXiv:2605.11043, 2026.

[21] Whiffen, G., Wallace, M., Landau, D., Pellegrini, E., Lantoine, G., Petropoulos, A., Choi, S., Anderson, B., Olikara, Z., and Sims, J. “GTOC13: Humanity’s First Robotic Exploration of a Hypothetical Exoplanetary System.”, 2025.

[22] Tsuda, Y., Mori, O., Funase, R., Sawada, H., Yamamoto, T., Saiki, T., Endo, T., and Kawaguchi, J. “Flight status of IKAROS deep space solar sail demonstrator.” Acta Astronautica, Vol. 69, No. 9, pp. 833–840, 2011. ISSN 0094-5765. doi:https://doi.org/10.1016/j.actaastro.2011.06.005.

[23] Johnson, L., Castillo-Rogez, J., and Lockett, T. “Near Earth asteroid Scout: Exploring asteroid 1991VG using a Smallsat.” “International Astronautical Congress,” MSFC-E-DAA-TN74034. 2019.

[24] Mansell, J. R., Bellardo, J. M., Betts, B., Plante, B., and Spencer, D. A. “LightSail 2 Solar Sail Control and Orbit Evolution.” Aerospace, Vol. 10, No. 7, p. 579, Jun. 2023. ISSN 2226-4310. doi:10.3390/aerospace10070579.

[25] Rogers, B. A., Hughes, K. M., Longuski, J. M., and Aldrin, B. “Establishing cycler trajectories between Earth and Mars.” Acta Astronautica, Vol. 112, pp. 114–125, Jul. 2015. ISSN 00945765. doi:10.1016/j.actaastro.2015.03.002.

[26] Chen, K. J., Rogers, B. A., Okutsu, M., Landau, D. F., and Longuski, J. F. “Low-thrust Aldrin cycler with reduced encounter velocities.” Journal of Spacecraft and Rockets, Vol. 49, No. 5, pp. 955–961, 2012.

[27] Vergaaij, M. and Heiligers, J. “Time-optimal solar sail heteroclinic-like connections for an Earth-Mars cycler.” Acta Astronautica, Vol. 152, pp. 474–485, Nov. 2018. ISSN 00945765. doi:10.1016/j.actaastro.2018.08.008.